

# Modeling and performance analysis of real-time BDS-3 PPP-B2b one-way timing with uncombined observations

WANG Yong<sup>1,2,3</sup>, LIU Tianjun<sup>1,2</sup>, GU Shengfeng<sup>1,2</sup>, GE Yulong<sup>4</sup>, JIANG Weiping<sup>1,2</sup>

(1. GNSS Research Center, Wuhan University, Wuhan 430079, China; 2. Hubei LuoJia Laboratory, Wuhan 430079, China; 3. Jiangsu Province Surveying and Mapping Engineering Institute, Nanjing 210013, China; 4. School of Marine Science and Engineering, Nanjing Normal University, Nanjing 210023, China)

**Abstract:** Currently, the BeiDou-3 (BDS-3) precise point positioning (PPP) service (PPP-B2b) mostly employs the ionosphere-free (IF) combination model for precise timing, which tends to amplify the noise in observation values. To address this issue, this paper proposes a real-time BDS-3 precise unidirectional timing model based on uncombined (UC) observations using the BDS-3 PPP-B2b service. This model resolves the challenge of the amplified observation noise inherent in the IF combination model. The experiment involved selecting eight global navigation satellite system (GNSS) observation stations within China and collecting continuous observation data for 15 d. A comparative analysis with the traditional dual-frequency IF combination PPP timing model showed that the BDS-3 UC PPP timing based on the BDS-3 PPP-B2b service can achieve a timing precision of 0.5 ns. In addition, it was found that due to global positioning system (GPS) satellite clock products in the BDS-3 PPP-B2b service not being unified to the standard time, the GPS IF PPP timing method based on the BDS-3 PPP-B2b service is not recommended for precise timing. In summary, the BDS-3 UC PPP timing model proposed in this paper is suitable for precise timing, providing observation values with smaller noise, and its timing accuracy is comparable to that of the BDS-3 IF PPP, with slightly better frequency stability.

**Key words:** precise point positioning service; precise timing; BDS-3; uncombined precise point positioning  
DOI:10.3969/j.issn.1003-7985.2025.01.009

High-precision time information plays an important role in communication, finance, and military applications<sup>[1]</sup>. Some infrastructure types, such as 5G com-

munication base stations and radar, also need high-precision and accurate time signals. Currently, global navigation satellite systems (GNSS) one-way timing technology is the main timing technology and is widely used. The timing work is broadcasting a standard time; hence, time users can obtain time signals from GNSS time directly, such as BeiDou (BDS) time or BDT, global positioning system (GPS) time or GPST, and Galileo system time or GST. At present, the traditional timing accuracy can achieve 20-50 ns with the single point positioning model; therefore, time users are increasingly concerned about GNSS time transfer methods with higher precision.

Subsequently, the common-view (CV) with GPS satellites, which can reach the level of a few nanoseconds, was officially used for universal time coordinated (UTC) comparison in 1980<sup>[2]</sup>. Meanwhile, the all-in-view (AV) has reached better time transfer since 2004 with the development of precise orbit and clock products: the time transfer with the AV technique is not limited by distance, and its performance is superior to the CV time transfer<sup>[3]</sup>. The CV and AV time transfer is usually used for GNSS pseudorange observations. Therefore, precise point positioning (PPP), using carrier phase and pseudorange observations, is investigated by many researchers for time transfer<sup>[4]</sup>. PPP is not limited by the distance between different users with a 0.3-ns precision level and is formally used in the UTC/TAI (international atomic time) comparison<sup>[5]</sup>. Subsequently, scholars have gradually carried out more in-depth research on the PPP time transfer. Tu et al.<sup>[6]</sup> studied the BDS-2 PPP time transfer with triple-frequency (TF) observations and presented that the TF PPP exhibited similar performance to the dual-frequency PPP model. Meanwhile, Zhang et al.<sup>[7]</sup> investigated the Galileo PPP time transfer using quad-frequency observations and suggested that these observations can enhance the reliability of PPP. Then, with users demanding real-time performance, the real-time PPP time transfer has been gradually explored. Defraigne et al.<sup>[8]</sup> have earlier studied the PPP time transfer and achieved the time transfer precision in subnanoseconds in real time. A clock model for PPP was proposed by Lü et al.<sup>[9]</sup>, which could improve the real-time PPP time transfer and reduce the reconvergence when the data is interrupted. More recently, preliminary studies on real-time

Received 2024-07-21, Revised 2024-09-30.

**Biographies:** Wang Yong (1978—), male, Ph. D. candidate, professor of engineering; Jiang Weiping (corresponding author), male, doctor, professor, wpjiang@whu.edu.cn.

**Foundation items:** The Basic Science Center Project of the National Natural Science Foundation of China (No. 42388102), the Jiangsu Province Natural Resources Science and Technology Project (No. JSZRKJ202404).

**Citation:** WANG Yong, LIU Tianjun, GU Shengfeng, et al. Modeling and performance analysis of real-time BDS-3 PPP-B2b one-way timing with uncombined observations[J]. Journal of Southeast University (English Edition), 2025, 41 (1): 67-77. DOI: 10.3969/j.issn.1003-7985.2025.01.009.

BeiDou-3 (BDS-3) PPP have been conducted by Ge et al.<sup>[10]</sup>, and they presented that it can achieve better than 1-ns time transfer precision.

Although the PPP time transfer has achieved high precision, it still requires data interaction without concealment and convenience; hence, real-time PPP timing came into being. For PPP timing, the satellite precision clock products play an important role in time information. Based on this background, Guo et al.<sup>[1]</sup> computed the datum of the satellite clock offset to the GNSS time system, and the PPP timing was then released. Wu et al.<sup>[11]</sup> presented a one-way timing service system based on UTC (NTSC). However, this PPP timing method relies on the internet to deliver real-time products, which will lead to PPP timing instability due to network communication problems. Fortunately, BDS-3 has provided the positioning, navigation, and timing service since July 31, 2020<sup>[12]</sup>, which features short-message communication<sup>[13]</sup> and PPP service via B2b signal from Geostationary Earth Orbit satellites<sup>[14]</sup>. Then, BDS-3 PPP was used for many fields using PPP-B2b, for example, precise positioning<sup>[15-16]</sup>, ocean positioning<sup>[15,17-18]</sup>, and time transfer<sup>[19]</sup>. BDS-3 PPP can reach high-precision positioning and time transfer in non-internet environments and remote places with PPP-B2b. A multitude of studies have been conducted on the time transfer of BDS-3 PPP based on the PPP-B2b service, and research indicates that it can achieve a time transfer precision of approximately 0.5 ns. However, the investigation of precise timing with the PPP-B2b service is limited. Currently, the BDS-3 PPP timing is mainly based on the ionosphere-free (IF) combination model, and there is no timing model based on the uncombined (UC) PPP model as of yet. The datum of the satellite clock in the PPP-B2b is aligned to BDT for BDS-3 and hence makes precise timing using the PPP-B2b possible. In addition, the traditional PPP timing was based on the IF combination, and the UC PPP timing method with the PPP-B2b has not been studied yet.

Here, a real-time UC PPP timing method is proposed with a subnanosecond level. The recovery of the orbit/clock and the PPP timing model with the PPP-B2b service will be presented, and the processing strategies and tests will be introduced. Then, the PPP timing with the PPP-B2b will be validated and studied. Finally, the conclusion will be presented.

## 1 Methods

The recovery of orbit/clock from the PPP-B2b is presented, followed shortly by the one-way timing using the PPP-B2b.

### 1.1 Recovery of orbit/clock

A precise orbit consists of the broadcast ephemeris and

PPP-B2b, which can be presented as follows<sup>[20]</sup>:

$$\begin{cases} \mathbf{Y}_{\text{pre}} = \mathbf{Y}_{\text{brd}} + (\mathbf{h}_r, \mathbf{h}_a, \mathbf{h}_c) \times \Delta \mathbf{C} \\ \Delta \mathbf{C} = [\Delta \mathbf{C}_r, \Delta \mathbf{C}_a, \Delta \mathbf{C}_c] \\ \mathbf{h}_r = \frac{\mathbf{R}}{|\mathbf{R}|} \\ \mathbf{h}_c = \frac{\mathbf{R} \times \dot{\mathbf{R}}}{|\mathbf{R} \times \dot{\mathbf{R}}|} \\ \mathbf{h}_a = \mathbf{h}_c \times \mathbf{h}_r \end{cases} \quad (1)$$

where  $\mathbf{Y}_{\text{pre}}$  is the precise orbit;  $(\mathbf{h}_r, \mathbf{h}_a, \mathbf{h}_c)$  refers to the transformation matrix;  $\mathbf{Y}_{\text{brd}}$  indicates the orbits with broadcast ephemeris;  $\Delta \mathbf{C}$  indicates the correction in the PPP-B2b service;  $(\Delta \mathbf{C}_r, \Delta \mathbf{C}_a, \Delta \mathbf{C}_c)$  is the correction at radio, along, and cross-direction, respectively; and  $\dot{\mathbf{R}}$  and  $\mathbf{R}$  represent the velocity and position for the satellite, respectively.

The recovery of the precise clock is presented as follows:

$$t_{\text{pre}}^s = t_{\text{brd}}^s - \frac{\Delta D}{c} \quad (2)$$

where  $t_{\text{pre}}^s$  indicates the precise clock;  $t_{\text{brd}}^s$  refers to the clock in the broadcast ephemeris;  $\Delta D$  is the clock correction;  $s$  indicates the satellite; and  $c$  represents the speed of light.

### 1.2 UC PPP timing model

The B1I/B3I for BDS was selected for PPP timing in this paper. The uncombined (UC) carrier phase and pseudorange observations can be read as follows:

$$\begin{cases} p_{r,B1I}^s = \rho_r^s + (dt_r + d_{r,B1I}) - (dt^s + d_{B1I}^s) + T_r^s + I_r^s + \xi_{r,B1I}^s \\ p_{r,B3I}^s = \rho_r^s + (dt_r + d_{r,B3I}) - (dt^s + d_{B3I}^s) + T_r^s + \gamma I_r^s + \xi_{r,B3I}^s \end{cases} \quad (3)$$

$$\begin{cases} l_{r,B1I}^s = \rho_r^s + dt_r - dt^s + T_r^s - I_r^s + \lambda_{B1I} (N_{r,B1I}^s + B_{r,B1I} + B_{B1I}^s) + \psi_{r,B1I}^s \\ l_{r,B3I}^s = \rho_r^s + dt_r - dt^s + T_r^s - \gamma I_r^s + \lambda_{B3I} (N_{r,B3I}^s + B_{r,B3I} + B_{B3I}^s) + \psi_{r,B3I}^s \end{cases} \quad (4)$$

where  $p_{r,B1I}^s$  and  $p_{r,B3I}^s$  refer to the B1I and B3I pseudorange observations, respectively;  $l_{r,B1I}^s$  and  $l_{r,B3I}^s$  indicate the carrier phase observations;  $\rho_r^s$  is the distance between the satellite and the station;  $s$  and  $r$  refer to the satellite and receiver, respectively;  $dt_r$  and  $dt^s$  present the receiver and satellite clock offset, respectively;  $T_r^s$  is the tropospheric delays;  $I_r^s$  demonstrates the ionospheric delay in the B1I frequency;  $f$  indicates the frequency;  $\lambda$  is the wavelength;  $d_{r,f}^s$  and  $d_{r,f}$  are the pseudorange hardware delay;  $B_{r,f}$  and  $B_f^s$  are the phase delays;  $\gamma = f_{B1I}^2/f_{B3I}^2$  is the corresponding frequency coefficient;  $N_{r,k}^s$  is the ambiguity for carrier phase;  $\psi_{r,k}^s$  and  $\xi_{r,k}^s$  are the carrier phase and pseudorange observation noise under different frequency  $k$ , respectively.

Since the BDS-3 satellite broadcast clock uses the B3I signal as the frequency reference, the BDS-3 satellite clock will absorb the B3I signal code hardware delay; hence, the BDS-3 satellite clock  $\delta\hat{t}_r^s$  and the receiver clock offset  $\delta\hat{t}_r$  can be rewritten as follows:

$$\begin{cases} \delta\hat{t}_r = dt_r + \alpha d_{r,B1I} + \beta d_{r,B3I} = dt_r + d_{IF} \\ \delta\hat{t}_r^s = dt_r^s + d_{B3I}^s \\ \alpha = \frac{f_{B1I}^2}{f_{B1I}^2 - f_{B3I}^2} \\ \beta = \frac{-f_{B3I}^2}{f_{B1I}^2 - f_{B3I}^2} \end{cases} \quad (5)$$

Then, Eqs. (3) and (4) can be rewritten as follows:

$$\begin{cases} p_{r,B1I}^s = \rho_r^s + \delta\hat{t}_r - \delta\hat{t}_r^s + T_r^s + (I_r^s + \beta DCB_{r,B1I/B3I}) - \\ \quad DCB_{B1I/B3I}^s + \xi_{r,B1I}^s \\ p_{r,B3I}^s = \rho_r^s + \delta\hat{t}_r - \delta\hat{t}_r^s + T_r^s + \gamma(I_r^s + \beta DCB_{r,B1I/B3I}) + \xi_{r,B3I}^s \end{cases} \quad (6)$$

$$\begin{cases} l_{r,B1I}^s = \rho_r^s + \delta\hat{t}_r - \delta\hat{t}_r^s + T_r^s - (I_r^s + \beta DCB_{r,B1I/B3I}) + \\ \quad \lambda_{B1I} \hat{N}_{r,B1I}^s + \psi_{r,B1I}^s \\ l_{r,B3I}^s = \rho_r^s + \delta\hat{t}_r - \delta\hat{t}_r^s + T_r^s - \gamma(I_r^s + \beta DCB_{r,B1I/B3I}) + \\ \quad \lambda_{B3I} \hat{N}_{r,B3I}^s + \psi_{r,B3I}^s \end{cases} \quad (7)$$

where  $DCB_{B1I/B3I}^s$  can be obtained from the PPP-B2b differential code bias corrections for frequencies B1I and B3I.

To verify the results of BDS-3 UC PPP one-way timing with the PPP-B2b, the traditional IF PPP timing method was also used in this paper. After applying the corresponding correction models and precise products, the code and carrier phase observations can be expressed<sup>[21]</sup> as follows:

$$p_{r,IF}^s = \rho_r^s + \delta\hat{t}_r - \delta\hat{t}_r^s + T_r^s + \alpha DCB_{B1I/B3I}^s + \xi_{r,IF}^s \quad (8)$$

$$l_{r,IF}^s = \rho_r^s + \delta\hat{t}_r - \delta\hat{t}_r^s + T_r^s + \lambda_{IF} \hat{N}_{r,IF}^s + \psi_{r,IF}^s \quad (9)$$

where IF indicates the IF PPP model.

After calibrating the hardware delay,  $D_u$  represents the difference between BDT and local time, which is written as follows:

$$D_u = t_{BDT} - t_{local} \quad (10)$$

where  $u$  refers to the user and  $t_{local}$  is the user time.

The diagram of PPP timing is shown in Fig. 1 with BDS-3. First, the BDS-3 observations and broadcasts and the PPP-B2b corrections were received by the user. Then, the precise orbit/clock is recovered. Third, by using the PPP engine, the user will calculate the difference, which can be obtained as shown in Eq. (10).

In addition, with the traditional weighting and considering the accuracy of the orbit/clock, the weight  $H$  can be written as follows:

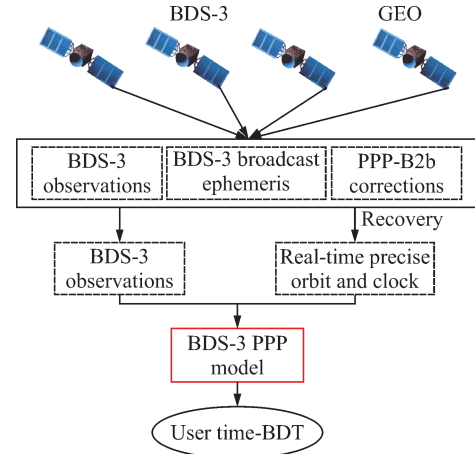


Fig. 1 Flowchart of one-way timing using the PPP-B2b

$$\begin{cases} H = \text{diag}(\sigma_1^{-2}, \sigma_2^{-2}, \dots, \sigma_m^{-2}) \\ \sigma^2 = GR_r(a_\sigma^2 + b_\sigma^2/\sin e^2) + \sigma_{\text{eph}}^2 \end{cases} \quad (11)$$

where  $G$  indicates the factor (BDS-3 : GPS = 1 : 1);  $b_\sigma$  and  $a_\sigma$  are carrier-phase error factors, which are set to 0.01 and 0.006 m, respectively;  $e$  indicates the elevation angle;  $R_r$  refers to the carrier phase/pseudorange error ratio (1/10 000);  $\sigma_{\text{eph}}$  refers to the user range accuracy from the PPP-B2b; and  $m$  represents the number of satellites.

### 1.3 PPP timing evaluation

The Allan variance is a time-domain method primarily used for assessing frequency stability. In this paper, the modified Allan variance is chosen as the evaluation method for time reference stability in the context of PPP timing. The formula for the modified Allan variance is as follows:

$$\sigma_y^2(\tau) = \frac{1}{2n^4(N-3n+2)} \sum_{j=1}^{N-3n+2} \left\{ \sum_{i=j}^{j+n-1} \left[ \sum_{k=i}^{i+n-1} (y_{k+n} - y_k) \right] \right\}^2 \quad (12)$$

where  $N$  represents the number of frequency bands,  $y_i$  is the observation value in the  $N$ -th frequency band, and  $n$  denotes the averaging factor, typically set as  $m=1$ . Then,

$$\sigma_x^2(\tau) = \frac{1}{2n^2(M-3n+2)\tau^2} \sum_{j=1}^{M-3n+1} \left[ \sum_{i=j}^{j+n-1} (x_{i+2n} - 2x_{i+n} + x_i) \right]^2 \quad (13)$$

where  $x_i$  represents phase observations. The distinction lies in the fact that the former uses frequency point observations as phase observations, with  $M = N + 1$ ,  $\tau = n\tau_0$  representing the average observation time interval, and  $\tau_0$  as the fundamental observation time interval.

## 2 Experiment and Data Description

To evaluate the efficiency of the BDS-3 UC PPP one-way timing with the PPP-B2b, seven stations from the MGEX and one station from the Jiangsu Continuous

Operational Reference System (CORS) in China were selected, namely BIK0, POL2, LCK4, JFNG, NSHD, GAMG, USUD, and CUSV. The processing strategies are then described.

## 2.1 Dataset

The test data were received from day of year (DOY) 103 to 117 in 2023. The PPP-B2b corrections were obtained from the CORS station located at Nanjing Normal University, China. In addition, the BDS-3 PPP with final products released from Wuhan University (WUM) was applied to assess PPP one-way timing with the PPP-B2b<sup>[22]</sup>.

## 2.2 Strategies

The dual-frequency IF or UC PPP one-way timing model was investigated. The detailed strategies of PPP one-way timing are presented in Table 1. Then, the relativistic Sagnac effect was corrected by the corresponding model, and tidal displacement was corrected by the IERS models<sup>[23]</sup>. Moreover, two schemes are designed. First, the BDS-3 IF PPP one-way timing with the PPP-B2b service was tested and analyzed. Second, the proposed BDS-3 UC PPP one-way timing with the PPP-B2b was presented and compared. In addition, the BDS-3 PPP with WUM products was set as the reference.

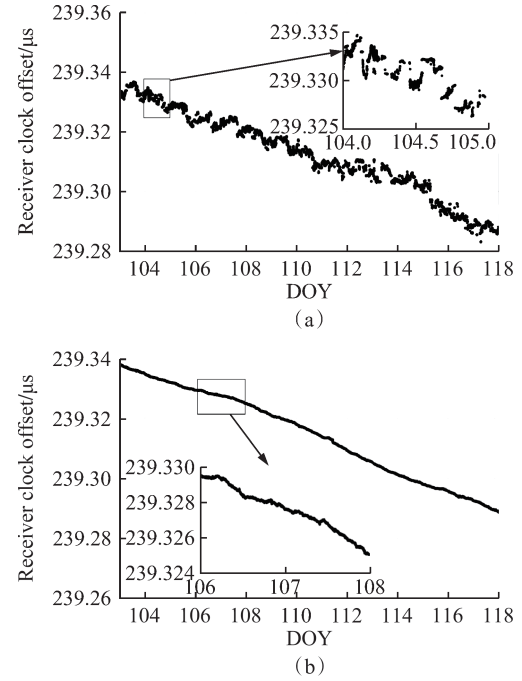
**Table 1** Strategies of PPP timing using the PPP-B2b

Parameters	Values
Estimator	Kalman
Signals	BDS-3: B1I/B3I GPS: L1/L2
PCV and PCO	"igs*.atx" file
Receiver clock offset	White noise ( $10^4$ m <sup>2</sup> )
Phase ambiguities	Estimated as constant
Precise products	CNAV1+ PPP-B2b correction WUM products <sup>[22]</sup>
Tropospheric delay	ZHD: corrected <sup>[24]</sup> ZWD: the random-walk model ( $5 \times 10^{-8}$ m <sup>2</sup> /s)
Tidal displacement	Corrected
Receiver coordinates	Estimated as constant

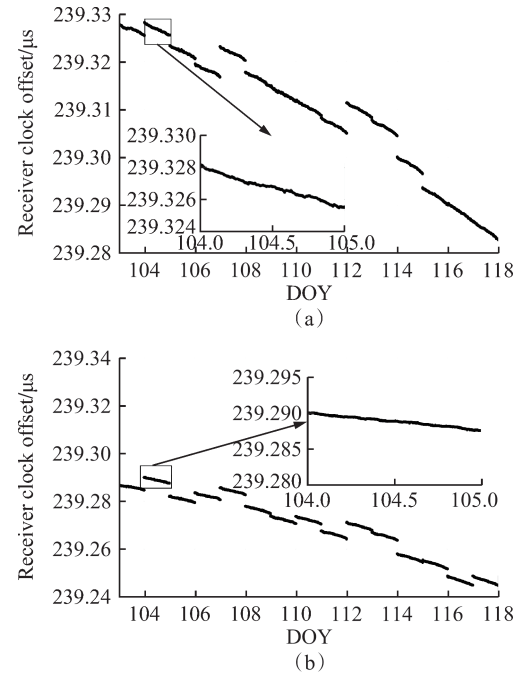
## 3 Result

Fig. 2 shows the receiver clock offset calculated from BDS-3 or GPS PPP with the PPP-B2b service at the USUD station. In addition, the receiver clock offsets of BDS-3 or GPS PPP using WUM products are shown in Fig. 3. Combined with the figures, two findings are presented. First, the GPS PPP solutions present a jumble of time series, as observed from the small zoom, whereas BDS-3 PPP solutions illustrate a continuous and stable time series. This may be explained by the fact that the datum of GPS in the PPP-B2b products is not aligned to a

uniform time datum<sup>[25]</sup>, whereas the reference of BDS-3 is BDT<sup>[14]</sup>. Hence, the PPP timing application with the PPP-B2b is not appropriate for using GPS satellites. Fortunately, BDS-3 PPP presents good performance for precise application with the PPP-B2b service and will be investigated and presented in this study. Second, as shown in Fig. 3, it can be concluded that the time series from BDS-3 or GPS PPP with the WUM products all exhibit obvious systematic bias between days and days, but they



**Fig. 2** Receiver clock offset obtained with the PPP-B2b service. (a) From GPS PPP; (b) From BDS-3 PPP



**Fig. 3** Receiver clock offset obtained with the WUM products. (a) From GPS PPP; (b) From BDS-3 PPP



are very stable within days. This may be because WUM products are not continuously estimated, and the daily benchmarks are not uniform. Fortunately, the datum of the satellite clock in the WUM product is stable and continuous; hence, the daily PPP solutions with WUM products were regarded as the true values.

Fig. 4 presents the receiver clock offset of four stations (i. e., GAMG, LCK4, USUD, and CUSV), which was calculated from the two BDS-3 PPP timing models. Four findings are explained in the following. First, an obvious phenomenon is that the receiver clock offset calculated by different stations presents different trends and noise phenomena, which may be because some stations use the frequency source provided by the internal crystal oscillator, such as the CUSV station, while some stations use high-performance atomic clocks, such as the cesium atomic clocks used by the USUD station. Second, there is a partial missing of the receiver clock offsets of

the CUSV station, which is caused by the missing observations of the CUSV station. Third, an important finding is that, from the perspective of the receiver clock difference time series calculated by the two models, the solutions of the two models are comparable, and there is no obvious systematic bias. This shows the feasibility of the UC PPP timing models. In addition, it can be proved from the model that the receiver clock offset from the BDS-3 UC PPP timing model includes the time difference between local time and BDT and the dual-frequency IF combination hardware delay (see Eqs. (3)-(5)). Fourth, from the receiver clock offsets of GAMG from the two BDS-3 PPP timing models, it can be observed that the noise obtained from the UC PPP timing model is smaller than that of IF PPP timing. This may be because the BDS-3 UC PPP timing model directly uses the original observations, whereas the BDS-3 IF PPP timing model amplifies the noise.

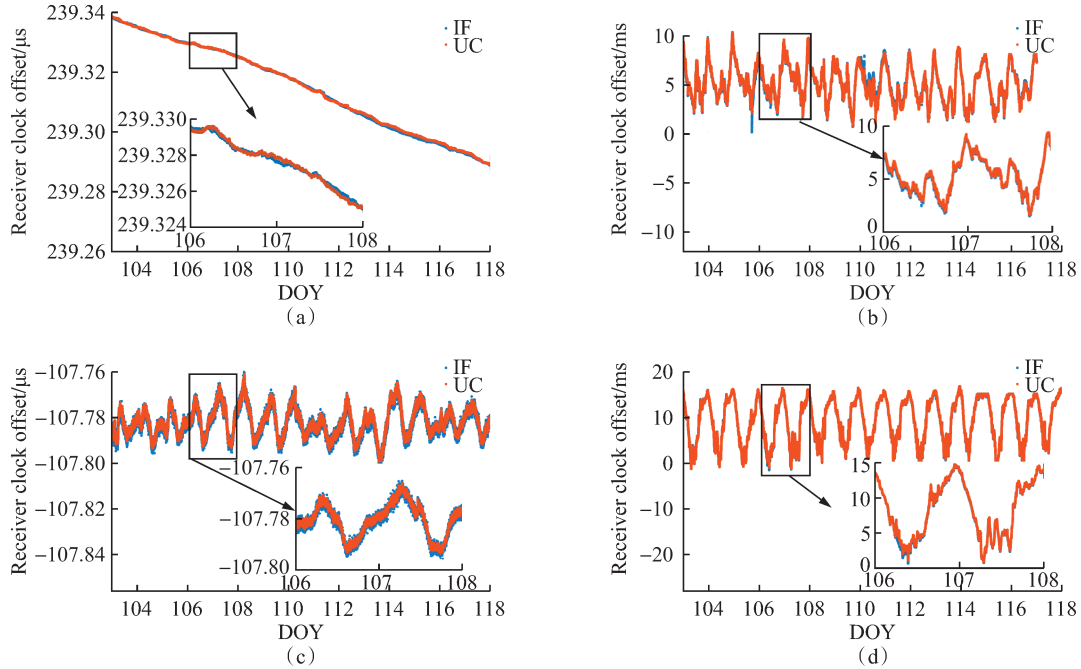


**Fig. 4** Receiver clock offset from two PPP models. (a) USUD; (b) CUSV; (c) GAMG; (d) LCK4

The clock differences between the two PPP timing models and PPP using WUM products are shown in Fig. 5 for seven stations. Note that IF and UC indicate the BDS-3 IF PPP timing model and the BDS-3 UC PPP timing model, respectively. Combined with the clock difference of seven stations, three conclusions can be drawn. First, as mentioned earlier, the datum of the satellite clock in WUM products has a significant system bias from day to day, but the datum of the satellite clock is stable in one day; hence, a one-day data arc is used to evaluate the two BDS-3 PPP timing models. Second, it can be easily seen that there was a significant reconvergence problem at the beginning of DOY 110, which was mainly due to the phenomenon of a short interruption in

the receiver at that time. Therefore, the reconvergence of PPP timing due to short-time outages caused by various factors still needs to be further resolved. Third, it was found that the timing solutions of the BDS-3 UC PPP timing model are basically in good agreement with the solutions of the BDS-3 IF PPP timing model and even better than that of the BDS-3 IF timing model. This phenomenon further confirms that the BDS-3 UC PPP model is suitable for timing applications and validates the advantages of the BDS-3 UC PPP timing model; that is, it directly uses the original observations.

To quantify the conclusion, the standard deviation (STD) and mean values of the clock difference between two BDS-3 PPP timing models with the PPP-B2b service

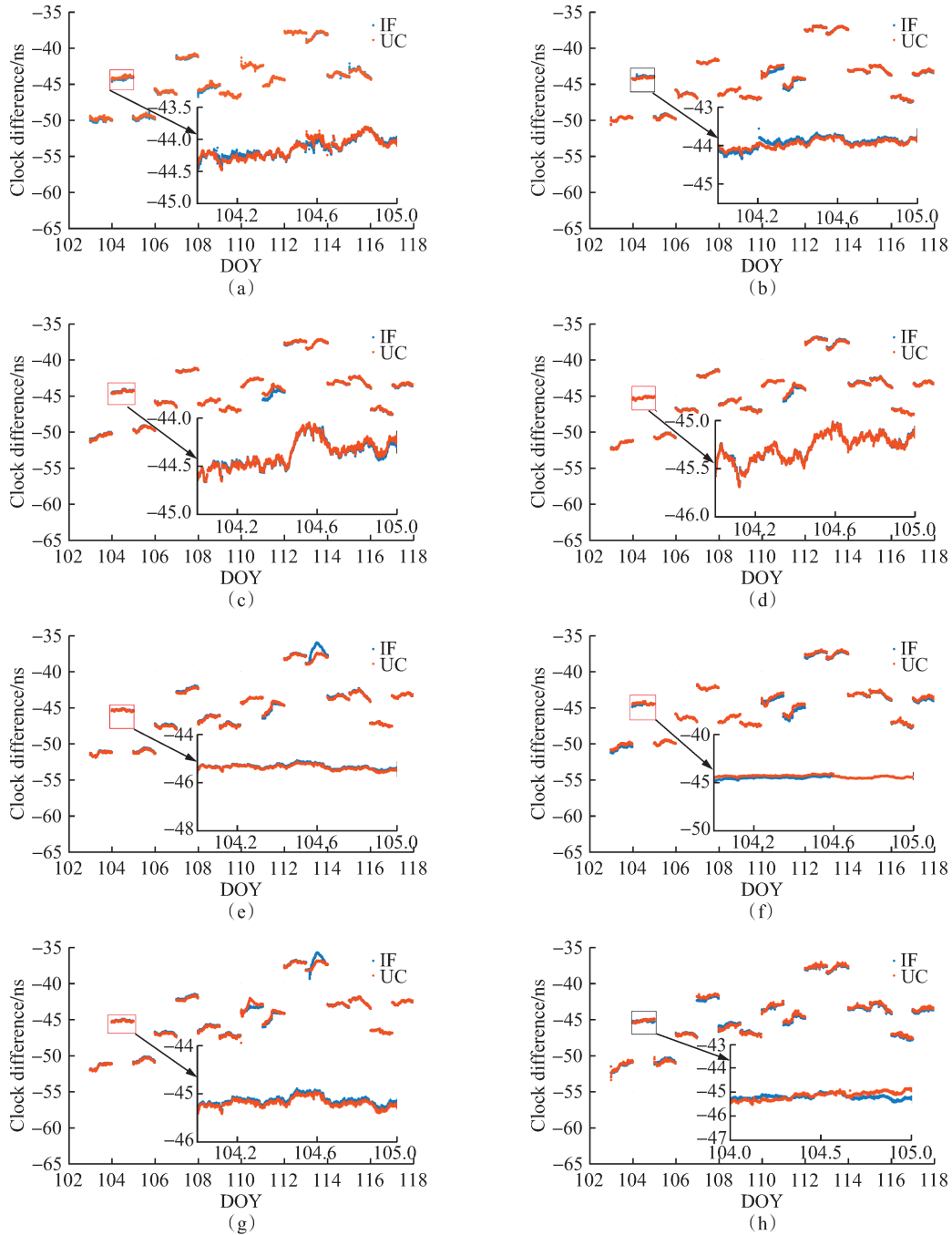


**Fig. 5** Clock differences between BDS-3 PPP using the PPP-B2b service and PPP with the WUM products. (a) CUSV; (b) GAMG; (c) JFNG; (d) LCK4; (e) POL2; (f) USUD; (g) BIK0; (h) BTLH

and BDS-3 PPP with the WUM products were calculated. The STD and mean values of the clock differences, which were calculated by the BDS-3 IF PPP timing model and the BDS-3 UC PPP timing model, for seven stations, are displayed in Fig. 6 and Fig. 7, respectively, on each day. The average STD values of the clock difference are calculated and presented in Table 2. Combining Fig. 6, Fig. 7, and Table 2, four findings are exhibited here. First, comparing the clock difference obtained by the BDS-3 IF PPP timing model and the BDS-3 UC PPP timing model, it can be seen that the clock difference solved by the two models does not show obvious

systematic deviation numerically, which is similar to the result theory obtained by the receiver clock offset sequence from earlier and further proves the feasibility of the BDS-3 UC PPP timing in Fig. 6. Second, except for the results of DOY 111 for all stations, the STD values of clock difference for other days can all satisfy better than 0.5 ns. Hence, it can be concluded that the precision of BDS-3 PPP timing with the PPP-B2b will reach the subnanosecond level, regardless of whether the BDS-3 IF PPP timing or the UC PPP timing is used. Third, in Table 2, the mean STD values for the two BDS-3 PPP timing models at NSHD, BIK0, CUSV,

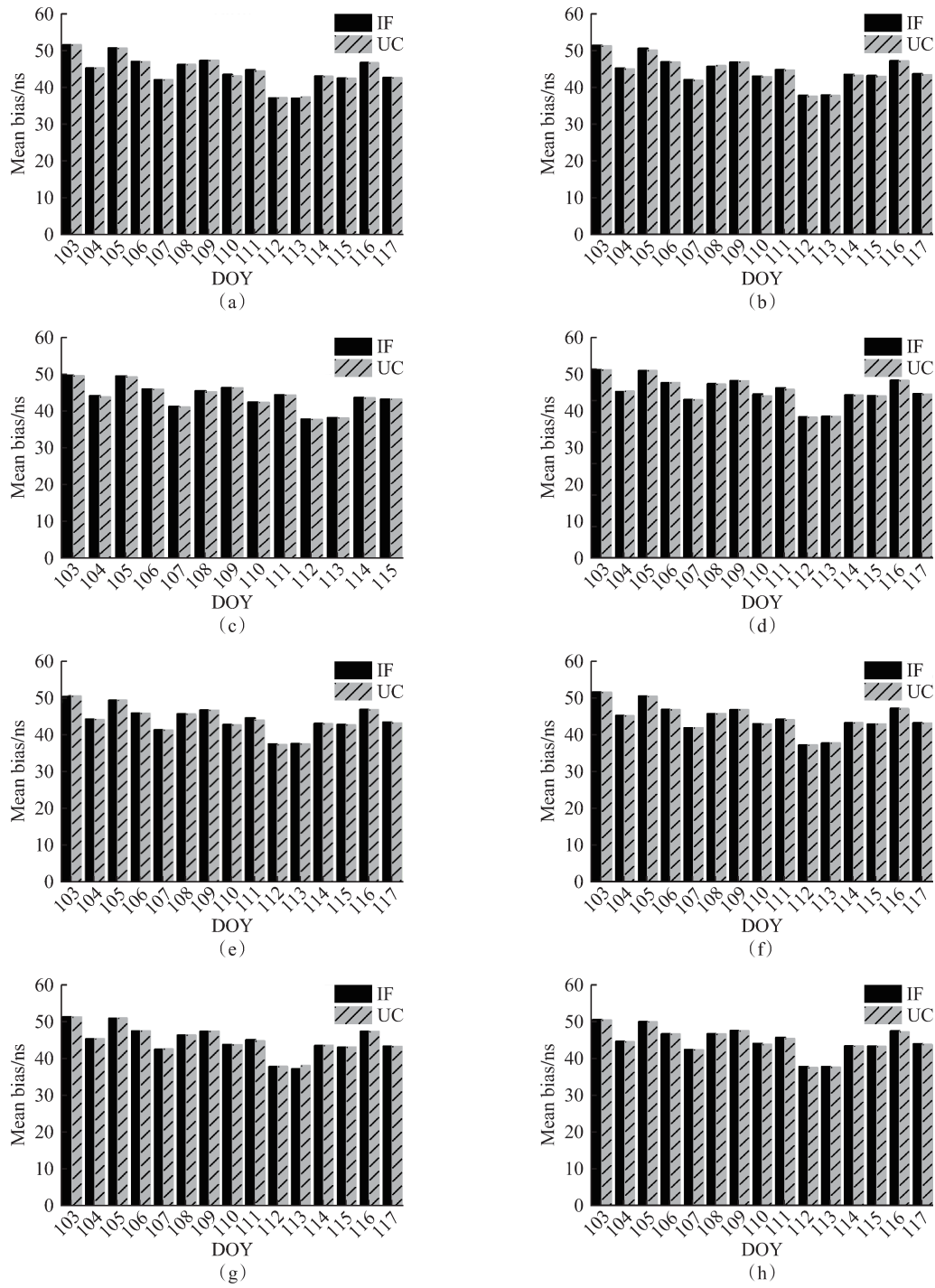


**Fig. 6** Mean bias of the clock difference between BDS-3 PPP using the PPP-B2b and PPP with WUM products. (a) BIK0; (b) BTLH; (c) CUSV; (d) GAMG; (e) JFNG; (f) LCK4; (g) POL2; (h) USUD

GAMG, JFNG, LCK4, POL2, and USUD stations are presented. Overall, the mean STD of the clock difference calculated by the two BDS-3 PPP timing models is less than 0.3 ns for all stations. Fourth, the precision of the UC PPP timing model is equal to or better than the IF PPP timing model with BDS-3 satellites, possibly because the BDS-3 UC PPP timing model uses the original observations and is less noisy than the BDS-3 IF PPP timing model.

To further evaluate the PPP timing performance and

compare the two PPP timing models, this paper further analyzed the frequency stability results. The modified Allan deviation (MDEV) of the PPP timing results for the two BDS-3 PPP timing models are presented in Fig. 8 and Fig. 9, respectively. Combining Fig. 8 and Fig. 9, three findings were drawn. First, from the point of view of frequency stability, the MDEVs of receiver clock offsets, which were obtained from the BDS-3 IF PPP timing model, for NSHD, BIK0, CUSV, GAMG, JFNG, LCK4, POL2, and USUD, are  $3.82 \times 10^{-12}$ ,  $7.05 \times$

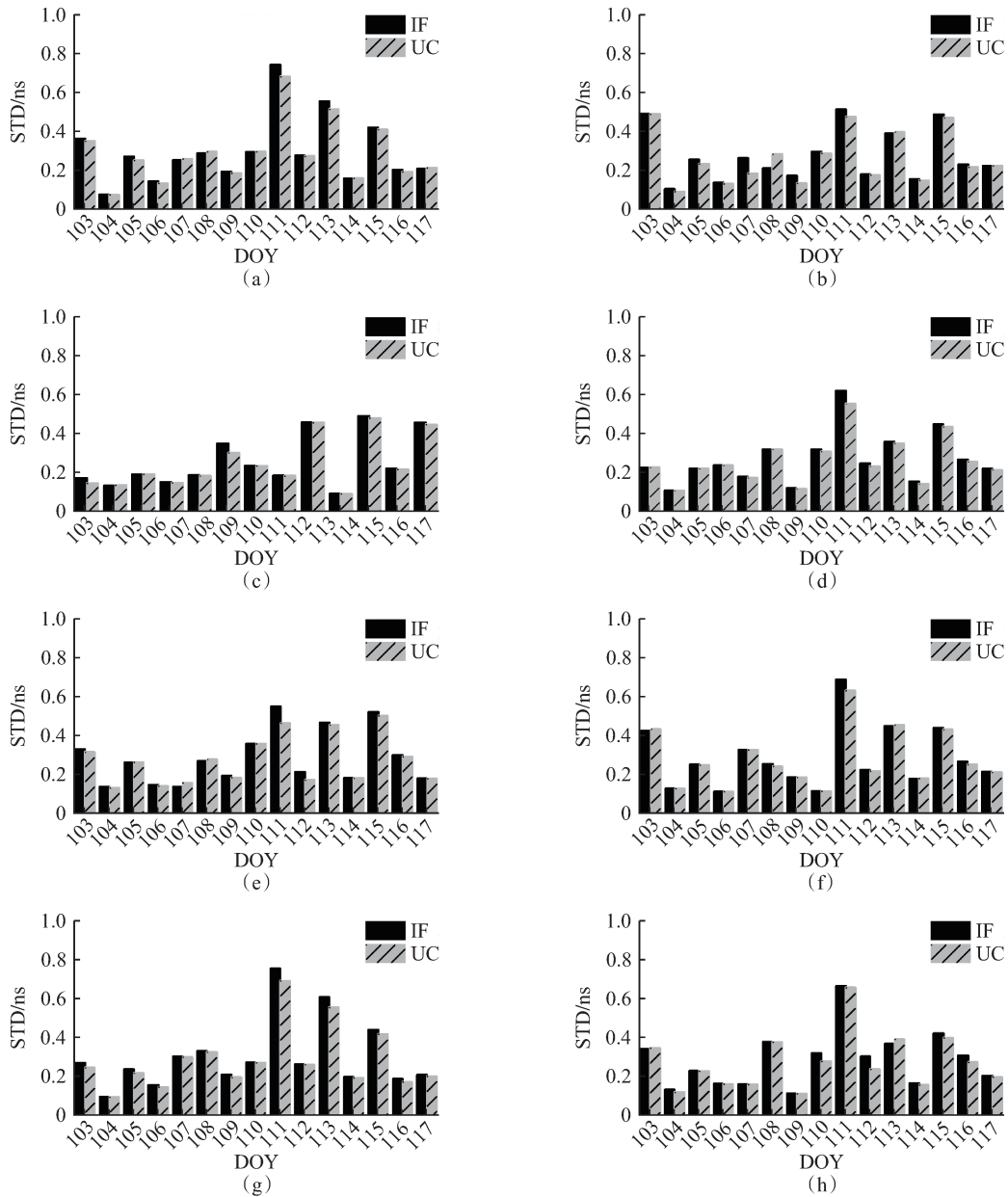


**Fig. 7** STD values of the clock difference between BDS-3 PPP using the PPP-B2b and PPP with WUM products. (a) BIK0; (b) BTJH; (c) CUSV; (d) GAMG; (e) JFNG; (f) LCK4; (g) POL2; (h) USUD

**Table 2** Mean STD of the difference between the two PPP timing models using the PPP-B2b service

Model	NSHD	BIK0	CUSV	GAMG	JFNG	LCK4	POL2	USUD
IF	0.27	0.30	0.25	0.27	0.28	0.28	0.30	0.28
UC	0.26	0.29	0.25	0.26	0.27	0.28	0.28	0.27

$10^{-13}$ ,  $2.47 \times 10^{-12}$ ,  $7.49 \times 10^{-13}$ ,  $2.58 \times 10^{-12}$ ,  $5.04 \times 10^{-12}$ ,  $1.67 \times 10^{-12}$ ,  $4.10 \times 10^{-14}$  at 960 s and  $1.41 \times 10^{-12}$ ,  $4.07 \times 10^{-13}$ ,  $1.39 \times 10^{-12}$ ,  $3.62 \times 10^{-13}$ ,  $3.65 \times 10^{-13}$ ,  $1.91 \times 10^{-12}$ ,  $5.85 \times 10^{-13}$ ,  $1.36 \times 10^{-14}$  at 15 360 s, respectively. The frequency stability of different stations shows different characteristics, which may be related to the performance of the atomic clock of each station. For example, the cesium atomic clock is connected to the

USUD station, and its frequency stability is significantly better than other stations. Second, the MDEVs of receiver clock offsets, which were obtained from the BDS-3 UC PPP timing model, for NSHD, BIK0, CUSV, GAMG, JFNG, LCK4, POL2, and USUD, are  $3.82 \times 10^{-12}$ ,  $7.05 \times 10^{-13}$ ,  $2.47 \times 10^{-12}$ ,  $7.49 \times 10^{-13}$ ,  $2.58 \times 10^{-12}$ ,  $5.04 \times 10^{-12}$ ,  $1.67 \times 10^{-12}$ ,  $4.10 \times 10^{-14}$  at 960 s and  $1.41 \times 10^{-12}$ ,  $4.07 \times 10^{-13}$ ,  $1.39 \times 10^{-12}$ ,  $3.62 \times 10^{-13}$ ,  $3.65 \times 10^{-13}$ ,  $1.91 \times 10^{-12}$ ,  $5.85 \times 10^{-13}$ ,  $1.36 \times 10^{-14}$  at 15 360 s, respectively. Based on the long- and short-term frequency stability, the frequency stability of solutions obtained from the BDS-3 UC PPP timing model is slightly better than the frequency stability of solutions calculated from the BDS-3 IF PPP timing model, which is similar to the previous conclusion.



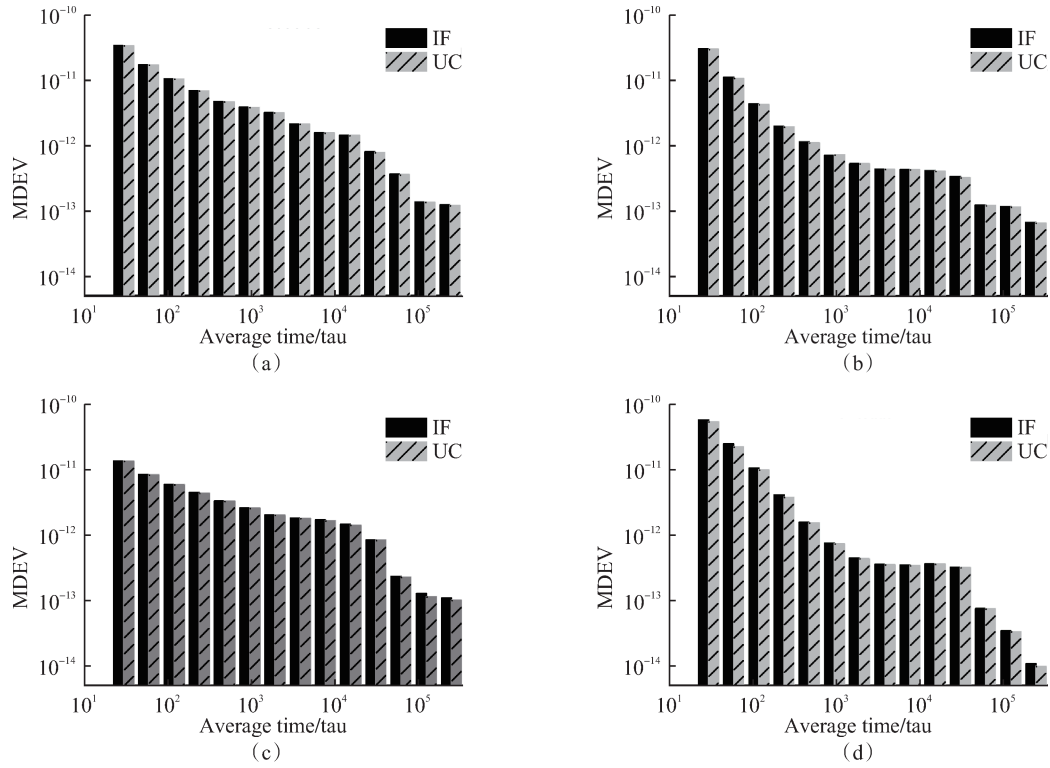


**Fig. 8** MDEV values of the receiver clock offsets obtained from the two PPP timing models for four stations. (a) BTLH; (b) BIK0; (c) CUSV; (d) GAMG

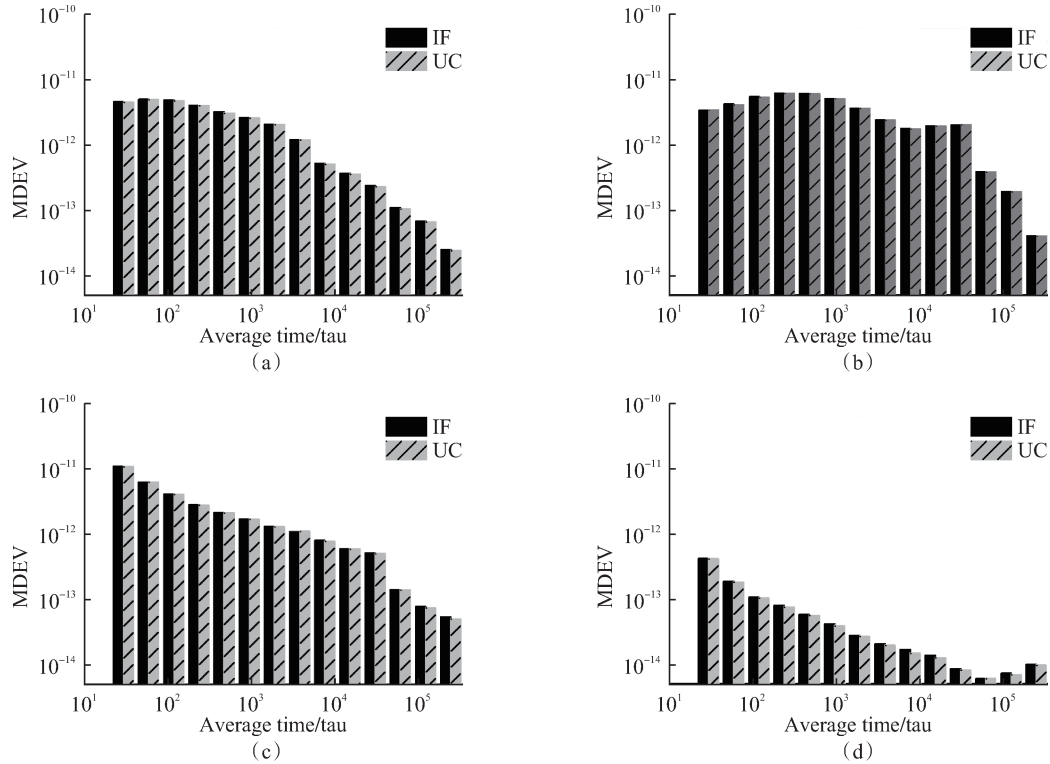


**Fig. 9** MDEV values of the receiver clock offsets obtained from the two PPP timing models for three stations. (a) JFNG; (b) LCK4; (c) POL2; (d) USUD

#### 4 Conclusions

Based on the results of this paper, three conclusions have been drawn as follows:

- (1) Due to the obvious jump in the receiver clock off-

set calculated by GPS PPP, because the time datum of the GPS clock in the PPP-B2b is not unified, it is difficult to realize the application of high-precision timing. The receiver clock offset of the traditional IF PPP is very continuous and stable because the datum of the BDS-3

clock in the PPP-B2b is BDT; hence, users can directly obtain synchronization with BDT through the BDS-3 IF PPP timing model. The precision of BDS-3 PPP one-way timing using the IF model will reach better than 0.5 ns.

(2) The timing solutions of the BDS-3 UC PPP model and the IF PPP model have no obvious systematic bias and are in good agreement, which also shows that the UC PPP model can be used in high-precision timing applications. The mean STD values of the clock difference between the timing results and the reference are 0.27, 0.30, 0.25, 0.27, 0.28, 0.28, 0.30, and 0.28 ns for the BDS-3 IF PPP timing model and 0.26, 0.29, 0.25, 0.26, 0.27, 0.28, 0.28, and 0.27 ns for the BDS-3 UC PPP timing model at NSHD, BIK0, CUSV, GAMG, JFNG, LCK4, POL2, and USUD stations, respectively.

(3) The short- and long-term frequency stability of solutions obtained from the BDS-3 UC PPP timing model is slightly better than that of the BDS-3 IF PPP timing model. In addition, the UC PPP timing model is more effective due to each independent frequency to form the observation equations.

## References

- [1] GUO W F, SONG W W, NIU X J, et al. Foundation and performance evaluation of real-time GNSS high-precision one-way timing system [J]. *GPS Solutions*, 2019, 23(1): 23.
- [2] ALLAN D W, WEISS M A. Accurate time and frequency transfer during common-view of a GPS satellite [C]//34th Annual Symposium on Frequency Control. Philadelphia, PA, USA, 2005: 334-346.
- [3] LEE S W, SCHUTZ B E, LEE C B, et al. A study on the common-view and all-in-view GPS time transfer using carrier-phase measurements [J]. *Metrologia*, 2008, 45(2): 156-167.
- [4] GE Y L, CAO X Y, ZHOU F, et al. An improved method for real-time PPP timing and time transfer with broadcast ephemerides [J]. *Measurement Science and Technology*, 2022, 33(10): 105121.
- [5] PETIT G. The TAIPPP pilot experiment [C]//2009 IEEE International Frequency Control Symposium Joint with the 22nd European Frequency and Time forum. Besancon, France, 2009: 116-119.
- [6] TU R, ZHANG P F, ZHANG R, et al. Modeling and performance analysis of precise time transfer based on BDS triple-frequency un-combined observations [J]. *Journal of Geodesy*, 2019, 93(6): 837-847.
- [7] ZHANG P F, TU R, GAO Y P, et al. Performance of Galileo precise time and frequency transfer models using quad-frequency carrier phase observations [J]. *GPS Solutions*, 2020, 24(2): 40.
- [8] DEFRAIGNE P, AERTS W, POTTIAUX E. Monitoring of UTC(k)'s using PPP and IGS real-time products [J]. *GPS Solutions*, 2015, 19(1): 165-172.
- [9] LÜ D Q, ZENG F L, OUYANG X F, et al. Enhancing multi-GNSS time and frequency transfer using a refined stochastic model of a receiver clock [J]. *Measurement Science and Technology*, 2019, 30(12): 125016.
- [10] GE Y L, CHEN S X, WU T, et al. An analysis of BDS-3 real-time PPP: Time transfer, positioning, and tropospheric delay retrieval [J]. *Measurement*, 2021, 172: 108871.
- [11] WU M F, SUN B Q, WANG Y X, et al. Sub-nanosecond one-way real-time time service system based on UTC [J]. *GPS Solutions*, 2021, 25(2): 44.
- [12] YANG Y X, GAO W G, GUO S R, et al. Introduction to BeiDou-3 navigation satellite system [J]. *Navigation*, 2019, 66(1): 7-18.
- [13] GU S F, GUO R X, GONG X P, et al. Real-time precise point positioning based on BDS-3 global short message communication [J]. *GPS Solutions*, 2022, 26(4): 107.
- [14] YANG Y X, DING Q, GAO W G, et al. Principle and performance of BDSBAS and PPP-B2b of BDS-3 [J]. *Satellite Navigation*, 2022, 3(1): 5.
- [15] ZHAO N N, JIANG R. Poisoning attack detection scheme based on data integrity sampling audit algorithm in neural network [J]. *Journal of Southeast University (English Edition)*, 2023, 39(3): 314-322.
- [16] GUO S S, YU X W, LONG F Y, et al. Combined filter method for weakening GNSS multipath error [J]. *Journal of Southeast University (English Edition)*, 2022, 38(2): 178-185.
- [17] GENG T, LI Z Q, XIE X, et al. Real-time ocean precise point positioning with BDS-3 service signal PPP-B2b [J]. *Measurement*, 2022, 203: 111911.
- [18] YU J, ZHANG L, WU M, et al. Two-stage attention for rapid underwater image enhancement [J]. *Journal of Southeast University (English Edition)*, 2023, 39(4): 410-415.
- [19] TANG J, LYU D Q, ZENG F L, et al. Comprehensive analysis of PPP-B2b service and its impact on BDS-3/GPS real-time PPP time transfer [J]. *Remote Sensing*, 2022, 14(21): 5366.
- [20] XU Y Y, YANG Y X, LI J L. Performance evaluation of BDS-3 PPP-B2b precise point positioning service [J]. *GPS Solutions*, 2021, 25(4): 142.
- [21] ZUMBERGE J F, HEFLIN M B, JEFFERSON D C, et al. Precise point positioning for the efficient and robust analysis of GPS data from large networks [J]. *Journal of Geophysical Research: Solid Earth*, 1997, 102 (B3): 5005-5017.
- [22] CHEN G, GUO J, GENG T, et al. Multi-GNSS orbit combination at Wuhan University: Strategy and preliminary products [J]. *Journal of Geodesy*, 2023, 97(5): 41.
- [23] PETIT G, LUZUM B. IERS conventions (2010), IERS technical note No. 36 [R]. Frankfurt am Main: Verlag des Bundesamts für Kartographie und Geodäsie, 2010.
- [24] SAASTAMOINEN J. Atmospheric correction for the troposphere and stratosphere in radio ranging satellites [M]//Henriksen S W, Mancini A, Chovitz B H, eds. *Geophysical Monograph Series*. Washington DC: American Geophysical Union, 2013: 247-251.
- [25] GE Y L, CAO X Y, LYU D Q, et al. An investigation of PPP time transfer via BDS-3 PPP-B2b service [J]. *GPS Solutions*, 2023, 27(2): 61.

## 基于非组合观测值的实时北斗三 PPP-B2b 单向授时模型建立与分析

王勇<sup>1,2,3</sup>, 刘天骏<sup>1,2</sup>, 辜声峰<sup>1,2</sup>, 葛玉龙<sup>4</sup>, 姜卫平<sup>1,2</sup>

(1. 武汉大学卫星导航定位技术研究中心, 武汉 430079; 2. 湖北珞珈实验室, 武汉 430079;

3. 江苏省测绘工程院, 南京 210013; 4. 南京师范大学海洋科学与工程学院, 南京 210023)

**摘要:** 目前北斗三号(BDS-3)精密单点定位服务大多采用无电离层(IF)组合模型进行精密授时, 易放大观测值噪声。为此, 本文基于非组合观测值的实时北斗三 PPP-B2b 服务, 建立了一种基于非组合(UC)观测值的实时 BDS-3 精密单向授时模型, 解决了 IF 组合模型存在的观测值噪声被放大的难题。试验选取了 8 个中国境内的 GNSS 观测站, 并采集了连续 15 d 的观测数据。与传统的双频无电离层组合 PPP 授时模型进行对比分析, 结果表明, 基于 BDS-3 PPP-B2b 服务的 BDS-3 UC PPP 授时可实现 0.5 ns 的授时精度。此外, 由于 BDS-3 PPP-B2b 服务中 GPS 卫星钟产品的基准未统一至标准时间, 基于 BDS-3 PPP-B2b 服务的 GPS IF PPP 授时方法不建议用于精密授时。总之, 本文提出的 BDS-3 UC PPP 授时模型适用于精密授时, 可提供更小噪声的观测值, 其授时精度与 BDS-3 IF PPP 相当, 且其频率稳定度稍优于 BDS-3 IF PPP。

**关键词:** PPP-B2b; 精密授时; 北斗三号; 非组合 PPP

**中图分类号:** P228.9